Hindawi
Advances in Polymer Technology
Volume 2022, Article ID 3837232, 7 pages
https://doi.org/10.1155/2022/3837232

Research Article

On the Network Strength of Meta-Aramid Fiber Suspension and Its Relationship to Formation

Jiulong Sha,[1] **Jiawen Gao**,[1] **Peiyao Wang**,[1,2] **Qiannan Zhang**,[1] **Xinyi Zhang**,[1] **Shunxi Song**,[2] **and Peng Lu**[1]

[1]*Guangxi Key Laboratory of Clean Pulp & Papermaking and Pollution Control, College of Light Industry and Food Engineering, Guangxi University, Nanning 530004, China*
[2]*College of Bioresources Chemical and Materials Engineering, Shaanxi University of Science & Technology, Xi'an 710021, China*

Correspondence should be addressed to Jiulong Sha; shalong910226@hotmail.com and Shunxi Song; 15829913710@163.com

Received 1 September 2021; Revised 9 December 2021; Accepted 20 December 2021; Published 12 January 2022

Academic Editor: Kinga Pielichowska

Because of poor surface hydrophilicity, meta-aramid fibers readily form flocs by intertwining or interlacing, and this severely affects the uniformity of meta-aramid paper. To investigate the flocculation mechanism of meta-aramid fiber suspensions, the critical flocculant concentration, shear, and compressive network strength of meta-aramid fiber suspensions were examined. A hand sheet former was used to study the influence of the yielding properties of suspensions on the uniformity of meta-aramid paper, and the relationship between the formation index and rheological properties was determined. The results showed that the critical gel concentration ranged from 0.37 to 0.68 g/L, which was much lower than that of plant fiber suspensions. In addition, the compressive yield stress (Py) and shear yield stress (τy) of the meta-aramid fiber suspensions were found to increase linearly and exponentially, respectively, with an increasing concentration, and the uniformity index of the paper sheets was found to depend on a power of $\tau y \cdot Py$. This provides an effective method for predicting paper sheet uniformity.

1. Introduction

Because of their excellent chemical and thermal stabilities, heat resistance, and mechanical strength, meta-aramid-paper-based materials have recently received considerable attention in high-end fields such as defense, power, and transportation. Their unique physical and structural features give them particularly beneficial tensile, electrical, and chemical properties, which have attracted significant attention in academia in several disciplines [1–3].

Meta-aramid-paper-based materials, which consist of meta-aramid short fibers and fibrids, are prepared using a wet-forming papermaking process. Compared with cellulosic fibers, aramid fibers are prone to flocculation because of their long length and poor surface hydrophilicity, and this severely affects the uniformity of aramid paper and limits the application of aramid-paper-based materials in relevant high-end fields. Hence, efforts have been made to improve the dispersion of fibers via fiber surface modification or by using polymer dispersion additives; fiber flocculation mechanism was investigated as well. Jia et al. [4] used plasma to modify aramid fibers, and the results showed that plasma treatment has a significant impact on the surface morphology and chemical composition of fibers. Li et al. [5] found that the number of polar groups on the aramid fiber surface increased and the wetting performance improved after high-energy gamma-ray radiation treatments. Liu et al. [6] modified the aramid fiber surface properties by using the Friedel–Crafts reaction and found that this method can increase the number of active groups on the fibers without reducing the tensile strength of the fibers. More recently, surface coating [7, 8], coupling-agent modification [9], and fluorination modification [10] have also been used to improve the surface activity of the aramid fibers. Enhanced surface activity promotes the dispersion of aramid fibers in water and improves the evenness of aramid paper to some extent.

Among the chemical, colloidal, and hydrodynamic properties of the pulp suspension, the latter (hydrodynamic)

Table 1: Basic physical parameters of meta-aramid fiber materials.

	Fiber length/mm	Fiber width/μm	Coarseness/mg·m^{-1}	Kink index/%	Curl index/%
Short fiber	5.923	15.4	0.1940	6.8	23.2
Fibrid	0.763	30.2	0.0703	47.0	18.4

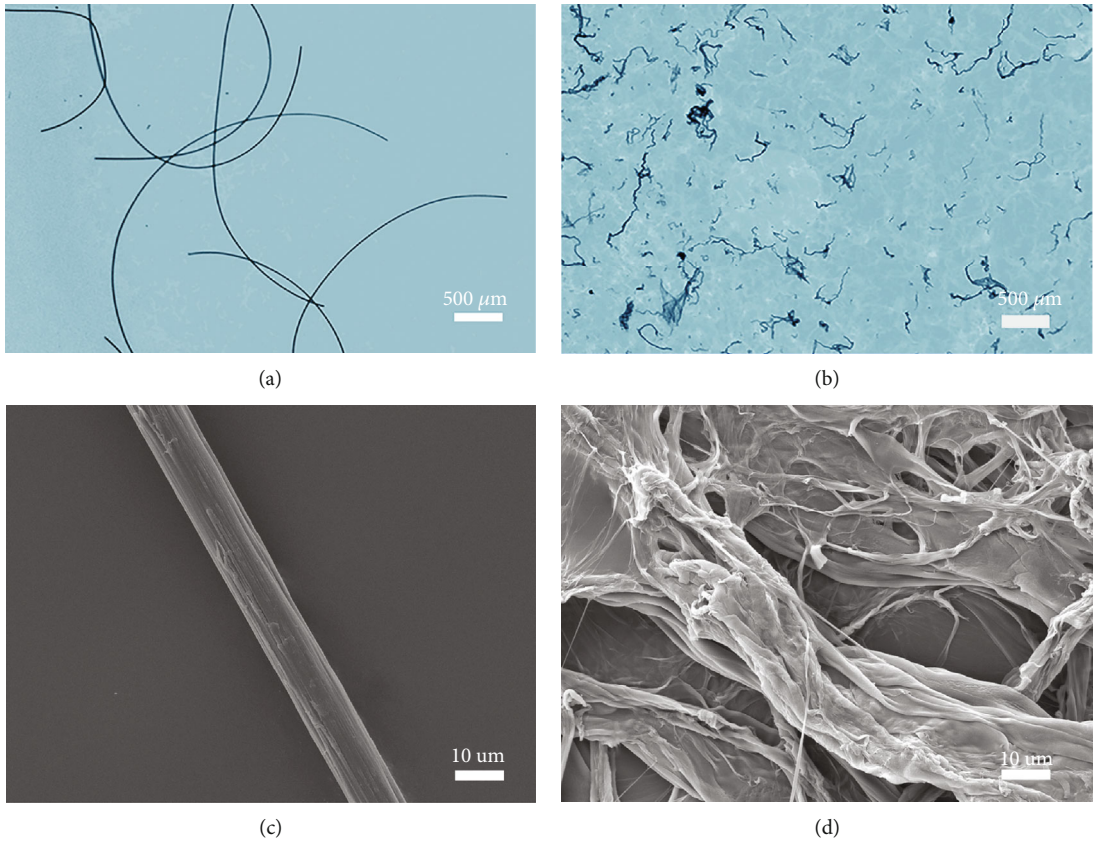

(a) (b) (c) (d)

Figure 1: Microscopic images of meta-aramid fiber: (a) short fiber; (b) fibrid and SEM images from surface: (c) short fiber and (d) fibrid.

plays a decisive role in the determination of the final sheet formation properties. To characterize the state of fiber flocculation and the probability of fibers forming flocs, Martinez et al. [11] identified a critical concentration, φg, also termed "gel point." It represents the lowest solids concentration at which fibers start to entangle and form interlocked networks having mechanical strength sufficient to overcome the external shear or compressive forces to maintain the stability of the fiber network structures.

As the concentration increases, the contact between individual meta-aramid fibers strengthens, and they entangle into rigid networks. Then, the structural strength of the fiber network can be characterized based on two types of stresses: compressive and shear yield stress. The compressive yield stress quantifies the network strength under compression; if the applied pressure load exceeds the network compressive yield stress, the fiber network collapses [12, 13]. The shear yield stress characterizes the structural stability of the fiber network under the shear flow field; to make the suspension flow, the shear yield stress must be overcome [14, 15]. During the wet-forming process, meta-aramid fiber suspension jets are impinged upon a moving wire, where water is drained to form a continuous web. The hydrodynamic flow of the suspensions imposes local pressure gradients that cause the deformation and rupture of the network flocs, resulting in an improved paper uniformity [16, 17]. Thus, the physical structure and yield stress of the fiber networks play a significant role in the determination of the final sheet quality.

In recent years, the shear and compressive network stress of pulp fiber suspensions have been extensively studied [18–20]. Despite the differences between the results of these studies, they all reported a significant concentration relationship.

$$\tau_y = a\varphi^b, \quad P_y = m\varphi^n. \tag{1}$$

Here, τy and Py represent the fiber–fiber contact stress, i.e., shear and the compressive yield stress (Pa), respectively, and a, b, m, and n are empirical parameters related to the

fiber properties. Derakhshandeh et al. [14] determined the yield stresses for commercial wood pulp suspensions by use of a conventional rheometer coupled with local velocity measurements (ultrasonic Doppler velocimetry), and ranges of a and b were reported to be 0.025-4.73 and 2.5-3.26, respectively. Sha et al. [21] measured the compressive yield stresses of acacia pulp fiber suspensions via equilibrium batch settling tests and the values of m and n were reported to be 9.19×10^{-6}-1.24×10^{-5} and 4.31-7.68, respectively.

Limited information is available on the rheology and dispersity of meta-aramid fiber suspensions. Thus, the objective of this study was to investigate the critical flocculant concentration, shear, and compressive yield stress of suspensions of the mixture of meta-aramid short fibers and fibrids, based on the rheological theory. Then, the influence of the yielding properties on the uniformity of meta-aramid paper sheets at low mass concentration was examined, and a model of the formation index and rheological properties was constructed. The results obtained may be used to increase the efficiency of the manufacturing process.

2. Experimental

2.1. Materials. Meta-aramid short fibers and fibrids were supplied by TayHo, Inc. (Yantai, China). The fiber morphologies were studied using a light microscope (MA410, Motic, China), and the fiber properties of each sample were measured using a Fibre Quality Analyzer (MorFi Compact, France). Before measurement, both raw materials were pretreated with a sodium dodecyl sulfate suspension at a concentration of 1.2×10^{-3} mol/L and stirred using a blender (PTI, Vorchdorf, Austria) for 30 min, to achieve complete mixing. The blender used an axial-flow impeller with a diameter of 4 cm, and a transparent cylindrical tank with a diameter of 30 cm and a height of 35 cm was used as a mixing vessel. The dispersed fibers were then washed with distilled water and dried in an oven at 105°C. Various short fiber/fibrid blends with ratios of 0/100, 20/80, 50/50, 80/20, and 100/0 were prepared and named SF0/100, SF20/80, SF50/50, SF80/20, and SF100/0, respectively.

2.2. Gel Point Measurements. Gel point was determined according to the sedimentation methodology described by Usher [15]. Five pulp suspensions with concentrations of 0.05, 0.10, 0.15, 0.20, and 0.25 g/L were prepared and transferred to 3000 mL graduated glass cylinders to study the settling behavior. The suspensions were allowed to settle for 10 h, and the sedimentation heights were recorded. The bottom pressure of the settling fiber network for each test cylinder, i, was calculated by using Equation (2) [20].

$$P_{\text{base},i} = \Delta\rho\varphi_{0,i}g/\rho_s. \quad (2)$$

The average solid concentration of the sediment at the bottom of each cylinder, i, can be simplified to

$$\varphi_{av,i} = \varphi_{0,i}h_{0,i}/h_{f,i}, , \quad (3)$$

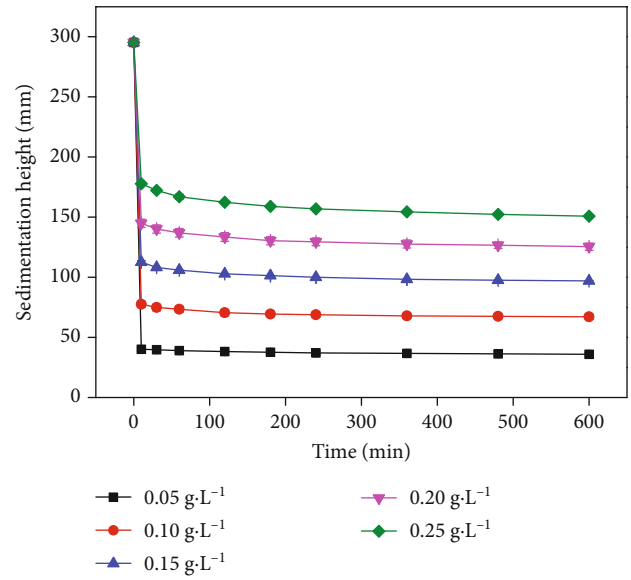

Figure 2: Sedimentation heights of aramid fiber suspensions (SF100/0, i.e., short fiber/fibrid = 1/0) at different initial concentrations as a function of time.

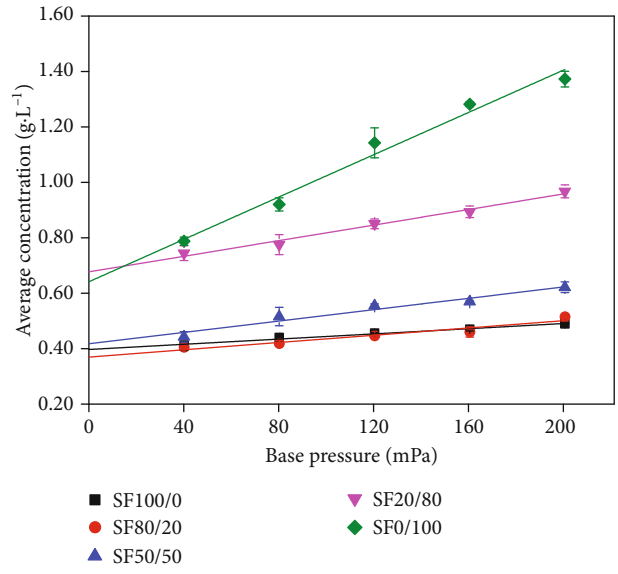

Figure 3: Average concentrations of aramid fiber sedimentation at different fiber/fibrid ratios as a function of base pressure.

where $\Delta\rho$ is the solid-liquid density difference (kg/m^3), g is the gravitational acceleration, $\varphi_{0,i}$ is the initial mass concentration (kg/m^3), $\rho_s$is the mass density of aramid fiber (1370 kg/m^3), and $h_{0.i}$and $h_{f,i}$ are the initial suspension height and final sediment height (m), respectively. The relationship between $\varphi_{av,i}$ and $P_{\text{base},i}$ was plotted, and a linear function was used to fit the curve; the intercept of the fit is the gel point value.

2.3. Compressive Yield Stress Measurements. The equilibrium sediment height data can be used to obtain the compressive yield stress value, $P_y(\varphi)$. For the mean final concentration

Table 2: Critical gel concentrations of aramid fiber suspensions with different fiber/fibrid ratios.

Sample	Average fiber length/mm	Coarseness/mg·m^{-1}	$\varphi_{av,i}$~$P_{base,i}$ fitting equation	R^2	Gel point/g·L^{-1}
SF100/0	5.923	0.1940	$Y = 4.71 \times 10^{-4}x + 0.40$	0.972	0.40
SF80/20	2.530	0.1386	$Y = 6.61 \times 10^{-4}x + 0.37$	0.909	0.37
SF50/50	1.292	0.1106	$Y = 10.3 \times 10^{-4}x + 0.42$	0.936	0.42
SF20/80	0.917	0.0775	$Y = 14.2 \times 10^{-4}x + 0.68$	0.979	0.68
SF0/100	0.763	0.0703	$Y = 38.4 \times 10^{-4}x + 0.64$	0.975	0.64

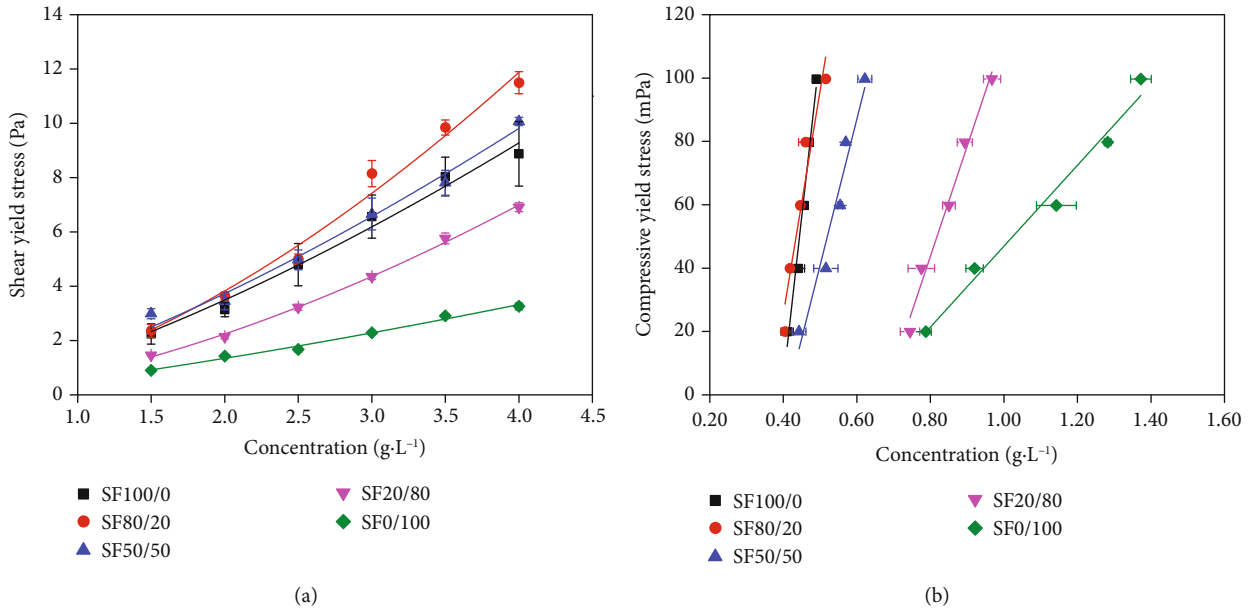

Figure 4: Yield stress values of aramid fiber suspensions as a function of concentration under (a) shear and (b) compression.

for each settling test,$\varphi_{av,i}$, the compressive yield stress can be determined by using the mean value approximation [19].

$$P_{y,i} = P_{base,i}/2. \tag{4}$$

Equations (3) and (4) were used to obtain a compressive yield stress datum point ($\varphi_{av,i}$,$P_{y,i}$), and then the mean value approximation was used to determine $P_y(\varphi)$. This process has been utilized in several other investigations; further details about compressive yield stress measurement are provided by Usher [19].

2.4. Shear Yield Stress Determination. Shear yield stress measurements were performed using a Brookfield RV30/60 system operating in controlled stress mode. The special geometry of the rotating blades of this measuring system has been determined to be superior to other geometries [21, 22], and it can help prevent sedimentation and wall slip effect. The rotor with four blades, 30 mm in diameter and 60 mm in height, was placed in a cylindrical cup with a diameter of 90 mm. The aramid fiber pulp was diluted with deionized water to prepare five 1000 mL suspension samples with concentrations of 1.5, 2.0, 2.5, 3.0, 3.5, and 4.0 g/L. To ensure the uniformity of initial conditions, all experimental samples were presheared at a fixed shear rate of 120 s^{-1} for 100 s and then rested for 30 s before testing. During the test, the samples were sheared for 30 s at a rotational speed of 10 r/min, and the maximum rotor torque was recorded. The peak torque during the shear test was converted to shear yield stress by using Equation (5) [23, 24]:

$$T_m = 1/2\pi D^3(H/D + 1/3)\tau_y, , \tag{5}$$

where T_m is the measured peak torque $(N \cdot m)$, and $D$and H are the diameter (m) and height of the vane (m), respectively. All tests were conducted at a temperature of 25°C.

2.5. Preparation of Aramid Paper. The traditional wet-forming papermaking process was adopted to prepare aramid paper. Fiber suspensions with different fiber/fibrid ratios are placed into a standard pulp homogenizer (L260-5011, Lorentzen&wettre, Sweden) for dispersion, and then the papers with a basis weight of 60 g/m^2 were manufactured using a sheet former (TD10-200R, Tongda Light Industry Equipment, Xianyang, China), followed by hot-pressing at 105°C for 8 min. Formation analysis of paper was accomplished by using a paper formation tester (Micro-Scanner, OpTest, Canada); the formation index revealed the local mass variations and network anisotropy.

Table 3: Fitting statistics of the yield stress of aramid fiber suspensions with various fiber/fibrid ratios.

Sample	τ_y~φ fitting equation	R^2	P_y~φ fitting equation	R^2
SF100/0	$Y = 1.32x^{1.41}$	0.980	$Y = 1038.78x - 411.22$	0.972
SF80/20	$Y = 1.23x^{1.63}$	0.980	$Y = 705.38x - 256.70$	0.909
SF50/50	$Y = 1.42x^{1.39}$	0.982	$Y = 461.45x - 189.83$	0.936
SF20/80	$Y = 0.72x^{1.64}$	0.998	$Y = 347.73x - 234.48$	0.979
SF0/100	$Y = 0.54x^{1.31}$	0.987	$Y = 127.69x$-80.78	0.975

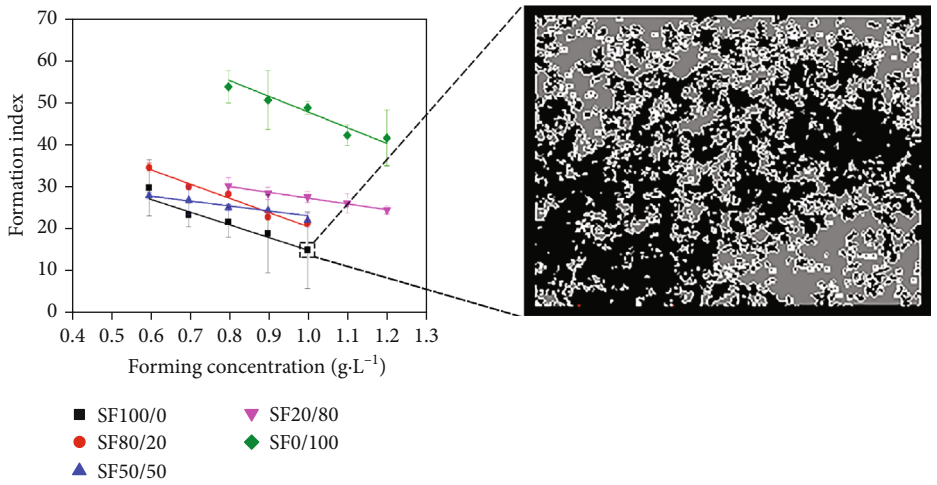

Figure 5: Formation index of meta-aramid papers with different fiber/fibrid ratios as a function of the formation concentration (the inset image shows a microscanned view of the aramid paper).

3. Result and Discussion

3.1. Morphological Properties. The fiber dimensions are summarized in Table 1. From Table 1, we can see that short fibers have a larger fiber length than those of fibrids and the fibrids present more kinks. The macroscopic morphology of meta-aramid short fibers and fibrids is presented in Figure 1. It can be observed that the short fibers are straight and have a smooth surface, whereas the fibrids are curled and have a rougher surface, which is favorable for the intersecting strength of aramid paper.

3.2. Gel Point. Figure 2 depicts the profiles of the settling interface of SF100/0 with time. With an increase in time, the sediment thickness of suspensions first decreases sharply and then stabilizes. This indicates that the fibers settle at high settling velocities during the initial period and eventually form packed sediment beds. With an increasing concentration, the equilibrium heights of the aramid fiber sediment increase exponentially. The experimental results suggest that the increased loading pressure on the network could cause an irreversible deformation of the network structures. Similar sedimentation behavior was observed for other pulp samples with different fiber/fibrid ratios.

The sedimentation behavior of fiber suspensions with different fiber/fibrid ratios was measured, and a datum point ($\varphi_{av,i}$, $P_{base,i}$) was determined using Equations (3) and (4). As shown in Figure 3, $\varphi_{av,i}$ increases linearly with the increase in $P_{base.i}$, a binary linear equation was used to fit the relationship, and the intercepts of fittings were used as the gel point values, φ_{gel}. The fitting constants for all test samples are summarized in Table 2.

As presented in Table 2, the gel point values of aramid fiber suspensions are in the range of 0.37–0.68 g/L; this means that aramid fibers can move freely, and no fiber flocs are formed below this critical concentration. In addition, at the proportions of short fibers above 50%, the gel point of the suspension decreases significantly. This was mainly attributed to the fact that the length of the short fibers are much greater than that of the fibrids, resulting in a greater probability of contact between fibers, making flocculation and entanglement easier. Moreover, the gel points of aramid fiber suspensions are considerably lower than those of natural wood pulp fiber suspensions (0.8–7.5 g/L) reported by Young et al. [25]. This indicates that the meta-aramid fibers are likely to flocculate at a lower concentration than plant fibers.

3.3. Yield Stress. Figure 4 shows the relationship between the shear and compressive network strength and the mass concentration of pulp suspensions. The shear yield stress increases exponentially from 0.9 to 11.5 Pa, whereas the compressive yield stress increases linearly from 19 to 100 MPa over the range of tested concentrations. Furthermore, the obtained yield stress values for aramid fiber suspensions are much higher than those for wood fiber

suspensions at the same concentration, indicating more stable and rigid network structures in aramid fiber suspensions [25]. However, the linear variation in the compressive yield stress is different from that reported in previous studies; this may be explained by the different particle species and dispersion solutions [12]. The results also showed that the compressive yield stress values are smaller by an order of magnitude, indicating that the network structure of aramid pulp fibers is more resistant to shear rather than compressive stress and has anisotropic properties.

As illustrated in Figure 4(a), compared with the SF0/100 samples, the shear yield stress of the mixed fiber suspensions increases with an increase in the short fiber/fibrid ratio, and the SF80/20 samples exhibit the maximum shear yield stress. However, there is a sudden decrease in the shear yield stress for the SF100/0 samples, and this could be explained by the lack of fibrids, which are favorable for the generation of cross-linking structures in the suspension, and hence, the shear strength of fiber networks decreases. Figure 4(b) shows that with the increase in the proportion of fibrids, the compressive yield stress of the pulps decreases at a certain concentration. As the proportion of short fibers decreases, the load-bearing capacity of the fiber network structure weakens and becomes more prone to collapse.

In addition, functions $\tau_y = a\varphi^b$ and $P_y = m\varphi$ were used to fit the curves, and the fitting statistics are summarized in Table 3. For all parameters, the coefficients of determination (R^2) are appropriate, indicating that the functional models fit the experimental data points well.

3.4. Sheet Formation Uniformity. The evenness of wet-forming paper is an important property for evaluating the final quality of paper, and it also affects the physical and chemical stability of paper. During the wet-forming process, shear and compression stresses are applied in the water medium flow field. Therefore, the coupling rheological effects of shear and compressive stresses influence the final uniformity of aramid papers.

Figure 5 shows the relationship between the evenness of sheets and concentration. The formation index of sheets decreases linearly as the fiber mass concentration increases, and the SF0/100 samples have the best paper uniformity, indicating that the fibers form more solid and nonuniform flocs with the addition of short fibers, leading to poor dispersion and reduced evenness of paper sheets.

To study the coupled effects of the compressive and shear yield stresses on the evenness of paper, the shear and compressive yield stress of aramid fiber suspensions were predicted according to the equation in Table 3 at mass concentrations ranging from 0.5 to 1.2 g/L; then, the relationship between the formation index of meta-aramid papers and$\tau_y \cdot P_y$ was obtained.

Figure 6 shows that the evenness of sheets decreases with the increase in $\tau_y \cdot P_y$, and all the formation index curves can be scaled together onto a single muster curve, indicating that all the aramid fiber suspensions likely follow the same sheet formation mechanism. At $\tau_y \cdot P_y < 0.1$ Pa^2, the formation index decreases sharply with the increase in $\tau_y \cdot P_y$, whereas above this critical value, the formation index decreases slightly. Such behavior may be attributed to the change in the interaction between fiber surfaces. With an increase in the suspension concentration, fibers become completely immobilized, interlocked, and in continuous contact, which significantly increases the network strength [15]. Thus, the type of fiber contact might influence the paper formation. Moreover, function $Y = 18.85x^{-0.21}$ fits the curve; the coefficient of determination (R^2) is 0.768. Thus, the formation index of meta-aramid papers can be predicted by an exponential function considering the shear and compressive network strength of the fiber suspensions.

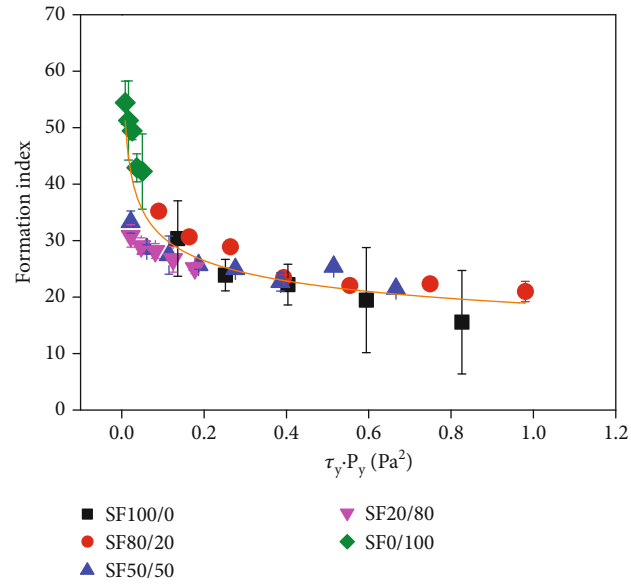

Figure 6: Formation index of meta-aramid papers as a function of $\tau_y \cdot P_y$.

4. Conclusion

The rheological behavior of aramid pulp fiber suspensions and the relationship between the yielding properties and sheet formation were studied. The results showed that the gel point values ranged from 0.37 to 0.68 g/L, and the minimum gel point value was achieved for the SF80/20 fiber samples, suggesting that they could reach the critical flocculation concentration more readily and form networks with higher strength compared with other samples. In general, the shear and compressive yield stress showed a strong dependency on concentration; their relationships followed a power-law and a linear dependency on the concentration, respectively. The experiments revealed that short fiber/fibrid ratio affected the dimensions of mixture fibers, thus impacting the fiber–-fiber interactions and yielding properties of pulp suspensions. As the concentration increased, the anisotropy of aramid papers increased; additionally, the formation index might be predicted based on $\tau_y \cdot P_y$ by using an exponential function.

Data Availability

The data used to support the findings of this study are available from the corresponding author upon request.

Conflicts of Interest

There are no conflicts to declare.

Acknowledgments

This research was supported by grants from the Natural Science Foundation of Guangxi (No. 2019GXNSFAA185010), the Open Foundation of Guangxi Key Laboratory of Clean Pulp & Papermaking and Pollution Control (No. 2019KF02), and the Scientific Research Foundation of Guangxi University (No. XJZ170390).

References

[1] W. Yang, X. Zhang, K. Yang et al., "Shear property characterization of aramid paper and its application to the prediction of honeycomb behaviors," *Composite Structures*, vol. 254, 2020.

[2] F. Xie, P. Qin, L. Zhuo, Z. Lu, and Y. Wang, "Novel aramid paper-based materials with enhanced thermal conductivity via ZnO nanowire decoration on aramid fibers," *Journal of Materials Science: Materials in Electronics*, vol. 29, no. 14, pp. 12161–12168, 2018.

[3] W. Zheng, J. Xie, J. Zhang, C. Tang, and Z. Zhao, "Influence of Polymethylsilsesquioxane Content to the Thermal Stability of Meta-Aramid Fiber Insulation Paper," *Materials*, vol. 11, no. 11, 2018.

[4] C. Jia, P. Chen, W. Liu, B. Li, and Q. Wang, "Surface treatment of aramid fiber by air dielectric barrier discharge plasma at atmospheric pressure," *Applied Surface Science*, vol. 257, no. 9, pp. 4165–4170, 2011.

[5] L. Xing, L. Liu, Y. Huang, D. Jiang, B. Jiang, and J. He, "Enhanced interfacial properties of domestic aramid fiber-12 via high energy gamma ray irradiation," *Composites Part B: Engineering*, vol. 69, pp. 50–57, 2015.

[6] T. Liu, Y. Zheng, and J. Hu, "Surface modification of Aramid fibers with new chemical method for improving interfacial bonding strength with epoxy resin," *Journal of Applied Polymer Science*, vol. 118, no. 5, pp. 2541–2552, 2010.

[7] L. Wang, Y. Shi, S. Chen et al., "Highly efficient mussel-like inspired modification of aramid fibers by UV-accelerated catechol/polyamine deposition followed chemical grafting for high-performance polymer composites," *Chemical Engineering Journal*, vol. 314, pp. 583–593, 2017.

[8] J. Zhu, L. Yuan, Q. Guan, G. Liang, and A. Gu, "A novel strategy of fabricating high performance UV-resistant aramid fibers with simultaneously improved surface activity, thermal and mechanical properties through building polydopamine and graphene oxide bi-layer coatings," *Chemical Engineering Journal*, vol. 310, pp. 134–147, 2017.

[9] Y. Ou, M. Lin, L. Su et al., "Highly mechanical nanostructured aramid-composites with gradient structures," *Composites Part A: Applied Science and Manufacturing*, vol. 118, pp. 250–258, 2019.

[10] H. Yuan, W. Wang, D. Yang et al., "Hydrophilicity modification of aramid fiber using a linear shape plasma excited by nanosecond pulse," *Surface and Coatings Technology*, vol. 344, pp. 614–620, 2018.

[11] D. M. Martinez, H. Kiiskinen, A. K. Ahlman, and R. J. Kerekes, "where p is the density of the suspension and U is a characteristic velocity. In subsequent work, changes in formation were measured as a function of," *Journal of Pulp and Paper Science: Transactions of the Technical Section*, vol. 29, p. 341, 2003.

[12] R. G. Kretser, D. V. Boger, and P. J. Scales, "Compressive rheology: an overview," in *Rheology reviews*, D. M. Binding and K. Walters, Eds., pp. 125–165, British Society of Rheology, Aberystwyth, 2003.

[13] M. S. Nasser, F. A. Twaiq, and S. A. Onaizi, "Effect of polyelectrolytes on the degree of flocculation of papermaking suspensions," *Separation and Purification Technology*, vol. 103, pp. 43–52, 2013.

[14] B. Derakhshandeh, S. G. Hatzikiriakos, and C. P. Bennington, "The apparent yield stress of pulp fiber suspensions," *Journal of Rheology*, vol. 54, no. 5, pp. 1137–1154, 2010.

[15] R. J. Kerekes, "Rheology of suspensions," *Nordic Pulp & Paper Research Journal*, vol. 21, no. 5, pp. 598–612, 2006.

[16] J. Zhao and R. J. Kerekes, "A historical perspective of scientific advances in paper forming hydrodynamics: 1950-2000," *BioResources*, vol. 12, no. 1, 2016.

[17] B. Nordström and L. Hermansson, "One-sided versus two-sided roll forming of never-dried softwood kraft pulp – effects on formation and strength efficiency," *Nordic Pulp & Paper Research Journal*, vol. 32, no. 3, pp. 407–414, 2017.

[18] B. Derakhshandeh, R. J. Kerekes, S. G. Hatzikiriakos, and C. P. J. Bennington, "Rheology of pulp fibre suspensions: A critical review," *Chemical Engineering Science*, vol. 66, no. 15, pp. 3460–3470, 2011.

[19] S. P. Usher, "Suspension Dewatering: Characterisation and Optimisation, [Ph.D. thesis]," The University of Melbourne, Melbourne, Australia, 2002.

[20] W. Li, Y. Yang, J. Sha, J. Zhou, C. Qin, and S. Wang, "The influence of mechanical refining treatments on the rheosedimentation properties of bleached softwood pulp suspensions," *Cellulose*, vol. 25, no. 6, pp. 3609–3618, 2018.

[21] J. Sha, Y. Yang, C. Wang et al., "The shear and compressive yield stress of fibrillated acacia pulp fiber suspensions," *Nordic Pulp & Paper Research Journal*, vol. 35, no. 2, pp. 243–250, 2020.

[22] W. K. J. Mosse, D. V. Boger, and G. Garnier, "Avoiding slip in pulp suspension rheometry," *Journal of Rheology*, vol. 56, no. 6, pp. 1517–1533, 2012.

[23] P. Estellé and C. Lanos, "Shear flow curve in mixing systems—A simplified approach," *Chemical Engineering Science*, vol. 63, no. 24, pp. 5887–5890, 2008.

[24] W. K. Mosse, D. V. Boger, G. P. Simon, and G. Garnier, "Effect of Cationic Polyacrylamides on the Interactions between Cellulose Fibers," *Langmuir*, vol. 28, no. 7, pp. 3641–3649, 2012.

[25] E. W. K. Young, D. M. Martinez, J. A. Olson et al., "The sedimentation of papermaking fibers," *AICHE Journal*, vol. 52, no. 8, pp. 2697–2706, 2006.